Journal of Biological Dynamics
Vol. 4, No. 5, September 2010, 506–526

Taylor & Francis
Taylor & Francis Group

The dynamics of an epidemic model with targeted antiviral prophylaxis

Zhipeng Qiu[a]* and Zhilan Feng[b]

[a]*Department of Applied Mathematics, Nanjing University of Science and Technology, Nanjing 210094, People's Republic of China;* [b]*Department of Mathematics, Purdue University, West Lafayette, IN 47907, USA*

(*Received 11 December 2009; final version received 25 May 2010*)

Due to the increasing risk of drug resistance and side effects with large-scale antiviral use, it has been suggested to provide antiviral drugs only to susceptibles who have had contacts with infectives. This antiviral distribution strategy is referred to as 'targeted antiviral prophylaxis'. The question of how effective this strategy is in infection control is of great public heath interest. In this paper, we formulate an ordinary differential equation model to describe the transmission dynamics of infectious disease with targeted antiviral prophylaxis, and provide the analysis of dynamical behaviours of the model. The control reproduction number $\mathcal{R}_c$ is derived and shown to govern the disease dynamics, and the stability analysis is carried out. The local bifurcation theory is applied to explore the variety of dynamics of the model. Our theoretical results show that the system undergoes two Hopf bifurcations due to the existence of multiple endemic equilibria and the switch of their stability. Numerical results demonstrate that the system may have more complex dynamical behaviours including multiple periodic solutions and a homoclinic orbit. The results of this study suggest that the possibility of complex disease dynamics can be driven by the use of targeted antiviral prophylaxis, and the critical level of prophylaxis which achieves $\mathcal{R}_c = 1$ is not enough to control the prevalence of a disease.

Keywords: epidemic model; targeted prophylaxis; reproduction number; bi-stability; bifurcation

AMS 2000 Mathematics Subject Classification codes: 92D30, 92D25, 34C25, 34C60

1. Introduction

Vaccination and antiviral drugs, along with non-pharmaceutical measures (case isolation, household quarantine, school or workplace closure, restrictions on travel), constitute a powerful line to defend against influenza outbreaks [9]. However, a vaccine can only protect against the strains of diseases that are expected to circulate in the next year. It is possible that a strain becomes common for which the vaccine does not provide protection since the virus changes rapidly. For example, in the 2003–2004 season, the vaccine did not protect against a predominant flu strain, A/Fujian

*Corresponding author. Email: nustqzp@mail.njust.edu.cn, smoller_1@163.com
Author Email: zfeng@math.purdue.edu

ISSN 1751-3758 print/ISSN 1751-3766 online

DOI: 10.1080/17513758.2010.498925
http://www.informaworld.com

[26]. Thus, antiviral drugs would be an attractive first line of defence in the first wave of pandemic infectious disease.

Antiviral drugs can be used to relieve the symptoms and lower infectiousness of the infected cases, and to prevent the suspectibles from being infected as well. For example, neuraminidase inhibitors and M2 inhibitors (adamantane derivatives) are two classes of antiviral drugs against influenza. The two classes of antiviral drugs can not only hasten infection clearance and lower infectiousness, but also reduce the probability that the suspectibles or exposed individuals infect with influenza [8]. Recently, there have been several literatures focusing on the impact of antiviral drugs as strategies for mitigating an influenza outbreak (see [10, 22] and references therein). Merler *et al.* [22] used a stochastic, spatially structured individual-based model to evaluate the efficacy of interventions based on the age-prioritized use of antiviral drugs, and Gani *et al.* [10] studied the potential impact of antiviral drug use during an influenza pandemic. However, widespread use of antiviral drugs has the potential to promote the emergence of resistant strains [21], and resistance to the antiviral drugs is more commonly associated with therapeutic than with prophylactic use [12]. Accordingly, the best use of these antiviral drugs would be prophylactic rather than therapeutic [18]. Since the use of antiviral drugs for prophylaxis is expensive, supplies will be limited, and prolonged use will increase the risk of side effects, antiviral drugs should be offered to susceptibles who have had contact with infectives. We will refer to this antiviral distribution strategy as 'targeted antiviral prophylaxis' [18]. Longini *et al.* [18] pointed out that targeted antiviral prophylaxis has potential as an effective measure for containing influenza until adequate quantities of vaccine are available. Hence, assessing the effectiveness and implications of the targeted prophylaxis intervention strategy can potentially help guide us to globally eliminate the infectious diseases and is of great public heath interest.

The use of mathematical models has proved a powerful tool for exploring the complex landscape of intervention strategies [9]. There have been several published mathematical models focused on exploring the impact of the various preventive and control strategies on transmission dynamics of the infectious diseases [2–4, 16, 20, 21, 23]. These models have provided many useful insights into preventing and containing the spread of the infectious diseases. Studies on mathematical models with targeted antiviral prophylaxis are also available in the literature. Longini *et al.* [18] used a stochastic epidemic simulation model to investigate the effectiveness of targeted antiviral prophylaxis to contain influenza. In 2005, Longini *et al*. [19] used an extension of the model in paper [18] to investigate the effectiveness of targeted antiviral prophylaxis, quarantine, and prevaccination on containing an emerging influenza strain at the source. McCaw and McVernon [20] developed novel deterministic models which introduce the contact class tracking the number of individuals in the population who have recently been in close contact with an infected person and who are therefore eligible to receive antiviral drugs as prophylaxis, and investigated the optimal use of an antiviral stockpile during an influenza pandemic. Soon after, McCaw *et al.* [21] extended the model formulated in paper [20] and considered the impact of emerging antiviral drug resistance on influenza containment and spread by using the extended model. Thieme *et al.* [24,25] studied a model, which is structured by a treatment age a, with targeted antiviral prophylaxis (referred to as treatment) under the assumptions that infected individuals who receive treatment do not transmit the disease, and that uninfected exposed individuals who receive treatment either have a reduced susceptibility (by a factor $q(a) \geq 0$) [24] or become permanently immune ($q = 0$) [25].

The purpose of this paper is to analyse the dynamics of an epidemic model with targeted antiviral prophylaxis. In this paper, we firstly formulate a model with targeted antiviral prophylaxis, which allows (i) a fraction of treated infectious individuals to transmit the disease; (ii) the possibility that for the fraction of treated infected individuals whose transmission was blocked, further infection may still occur if they continue to have contacts with infectious individuals; and (iii) treated individuals (either infected or uninfected) may lose their immunity. We then studied the mathematical properties of the model both analytically and numerically. Threshold conditions are

derived in terms of key parameters such as the treatment fraction f and the reduction of susceptibility in treated uninfected individuals γ. These conditions are shown to determine qualitative behaviours of the model. It is shown that multiple endemic equilibria exist in a certain parameter region, and that an endemic equilibrium may exist even when the reproduction number is less than one.

The local bifurcation theory is applied to prove that the system may undergo multiple Hopf bifurcations which lead to the appearance of two concentric limit cycles. The rich variety of dynamics of the system is also confirmed by numerical simulations. Our numerical results not only confirm the stability switches of the endemic equilibria, leading to the appearance of two periodic orbits, but also suggest the existence of a homoclinic orbit.

It is significant to point out that in the absence of targeted antiviral prophylaxis, our model reduces to a standard SIRS model, which has much simpler dynamics (e.g. there is no Hopf bifurcation or homoclinic orbit, and the endemic equilibrium is unique). This suggests that the introduction of targeted antiviral prophylaxis is responsible for the complex disease dynamics.

The paper is organized as follows. In Section 2, we introduce the model that incorporates targeted antiviral prophylaxis. Section 3 includes the derivation of the control reproductive number $\mathcal{R}_c$ and a detailed classification of the equilibria of the system. In section 4 we present a bifurcation analysis including stability switches and the appearance of periodic solutions. Section 5 is devoted to the numerical study of the system, which confirms/extends our theoretical results and illustrates the possible existence of a homoclinic orbit. The paper ends in section 6 with a discussion of the results.

2. Model description

The total population (N) is divided into five epidemiological classes: susceptible (S), treated (or prophylaxed) (P), untreated infectious (I_U), treated infectious (I_P), and recovered (R). A transmission diagram of the model is shown in Figure 5.

Assume that there is a constant recruitment rate Π into the susceptible class, and that there is a constant *per capita* natural death rate μ. The forces of infection for susceptibles (S) from untreated and treated infectious individuals are respectively

$$\lambda_U(t) = \beta k \frac{I_U}{N} \quad \text{and} \quad \lambda_P(t) = \delta\beta k \frac{I_P}{N}, \tag{1}$$

where k denotes the average number of contacts per individual per unit of time, β denotes the probability that an infection occurs per contact, and δ represents a reduction in the infectiousness in treated individuals. The rates at which susceptibles are exposed but uninfected, from contacts with untreated and treated individuals, are

$$\lambda_U^*(t) = (1-\beta) k \frac{I_U}{N} \quad \text{and} \quad \lambda_P^*(t) = (1-\delta\beta) k \frac{I_P}{N}, \tag{2}$$

respectively. Assume that a fraction f of all exposed individuals will receive prophylaxis. Then, the rate at which susceptibles are moved into the P class due to treatment is

$$f[\lambda_U^*(t) + \lambda_P^*(t)].$$

For those exposed infected individuals who are treated, the transmission can be blocked with probability c, in which case they will be moved into the P class at the rate $fc[\lambda_U(t) + \lambda_P(t)]$. The rest of the newly infected individuals (from the susceptible class) will enter the infectious

untreated class (I_U) at the rate $(1-f)[\lambda_U(t)+\lambda_P(t)]$ and will enter the infectious treated class (I_P) at the rate $f(1-c)[\lambda_U(t)+\lambda_P(t)]$. Since prophylaxis does not provide complete protection against the infection, individuals in the treated uninfected class (P) can still become infected (in this paper, we refer to this as reinfection) at a possibly reduced rate. Let $1-\gamma$, $0 \le \gamma < 1$, represent the level of protection by prophylaxis (i.e. $\gamma = 1$ for no protection and $\gamma = 0$ for complete protection), then the infection rate for individuals in the P class is $\gamma[\lambda_U(t)+\lambda_P(t)]$ (for ease of reference, we refer to this as reinfection and γ as reinfection coefficient). A treated individual returns to the susceptible class at the rate σ. An infected individual in the (I_U) and (I_P) class recovers at the rate η and $\theta\eta$, respectively. Here, $\theta \ge 1$, or $0 \le 1/\theta \le 1$ represents the reduction in infectious period due to treatment. A recovered individual may lose immunity at the rate ω ($\omega = 0$ represents the case of permanent immunity). Under the assumption of exponentially distributed stage durations, $1/\eta$ represents the average infectious period absent of treatment, and $1/\omega$ and $1/\sigma$ represent the average durations of immunity acquired from infection and prophylaxis, respectively. All parameters are non-negative.

Let

$$\lambda(t) = \lambda_U(t) + \lambda_P(t) \quad \text{and} \quad \lambda^*(t) = \lambda_U^*(t) + \lambda_P^*(t). \tag{3}$$

Based on the transfer diagram in Figure 1, our model consists of the following ordinary differential equations:

$$\begin{cases} S' = \Pi - [\lambda(t) + f\lambda^*(t)]S - \mu S + \omega R + \sigma P, \\ P' = fc\lambda(t)S + f\lambda^*(t)S - \gamma\lambda(t)P - (\sigma+\mu)P, \\ I_U' = (1-f)\lambda(t)S - (\eta+\mu)I_U, \\ I_P' = f(1-c)\lambda(t)S + \gamma\lambda(t)P - (\theta\eta+\mu)I_P, \\ R' = \eta I_U + \theta\eta I_P - (\mu+\omega)R. \end{cases} \tag{4}$$

All parameters are described above and summarized in Table 1.

Although some analytical results, in addition to numerical simulations, for the full system (4) will be obtained in the following sections, most of the analytical results will be derived for a reduced system, in which treated and untreated individuals are assumed to have the same transmission and recovery rates, i.e. $\delta = \theta = 1$. In this case, by letting $I = I_U + I_P$, the system (4) reduces to

$$\begin{cases} S' = \Pi - [\tilde{\lambda}(t) + f\tilde{\lambda}^*(t)]S - \mu S + \omega R + \sigma P, \\ P' = fc\tilde{\lambda}(t)S + f\tilde{\lambda}^*(t)S - \gamma\tilde{\lambda}(t)P - (\sigma+\mu)P, \\ I' = (1-fc)\tilde{\lambda}(t)S + \gamma\tilde{\lambda}(t)P - (\eta+\mu)I, \\ R' = \eta I - (\mu+\omega)R, \end{cases} \tag{5}$$

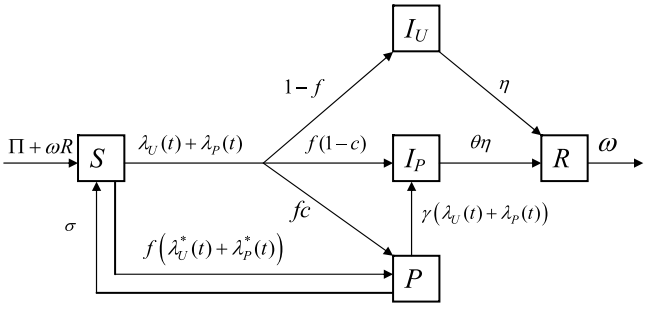

Figure 1. Disease transmission diagram of the model. The natural death rate from each class is not shown. All rates are per capita except ωR, which represents the rate at which recovered individuals becomes susceptible again after losing immunity.

Table 1. Definitions of frequently used symbols.

Parameter	Description
$S(t)$	Number of susceptible individuals at time t
$P(t)$	Number of treated (prophylaxed) individuals at time t
$I_U(t)$	Number of untreated infectious individuals at time t
$I_P(t)$	Number of treated infectious individuals at time t
$R(t)$	Number of recovered individuals at time t
$x(t)$	Fraction of susceptible individuals at time t
$y(t)$	Fraction of infectious individuals (untreated and treated) at time t
$z(t)$	Fraction of recovered individuals at time t
Π	Recruitment rate of individuals
$1/\mu$	Average life-span
$1/\omega$	Period of immunity acquired by infection
$1/\sigma$	Average time of losing drug-induced protection
k	Number of contacts per individual per unit time
β	Probability of becoming infected per contact
δ	Reduction factor in infectiousness due to the antiviral treatment
$1/\eta$	Infectious period of untreated individuals
$1/\theta$	Reduction in infectious period from treatment
c	Probability that transmission is blocked in an infected individual due to treatment
f	Proportion of exposed individuals that receive prophylaxis
γ	Relative susceptibility due to administration of prophylaxis

where

$$\tilde{\lambda}(t) = \beta k \frac{I}{N} \quad \text{and} \quad \tilde{\lambda}^*(t) = (1-\beta)k\frac{I}{N}. \tag{6}$$

Notice that the total population size N satisfies the equation

$$N' = \Pi - \mu N,$$

and that $N(t) \to \Pi/\mu$ as $t \to +\infty$. Thus, the biologically feasible region for system (7) is

$$\Gamma = \left\{(S, P, I, R) : 0 \le S, P, I, R, S + P + I + R = \frac{\Pi}{\mu}\right\},$$

which is positively invariant. We will restrict our attention to model behaviours in Γ and assume that the total population has stabilized at $N = \Pi/\mu$. In this case, it is easier to use fractions

$$x = \frac{S}{N}, \quad y = \frac{I}{N}, \quad z = \frac{R}{N},$$

and

$$w = \frac{P}{N} = 1 - x - y - z,$$

and thus, system (5) is equivalent to the following three-dimensional system:

$$\begin{cases} x' = \mu - [\tilde{\lambda}(t) + f\tilde{\lambda}^*(t)]x - \mu x + \omega z + \sigma(1 - x - y - z), \\ y' = (1 - fc)\tilde{\lambda}(t)x + \gamma\tilde{\lambda}(t)(1 - x - y - z) - (\eta + \mu)y, \\ z' = \eta y - (\mu + \omega)z. \end{cases} \tag{7}$$

where $\tilde{\lambda}(t)$ and $\tilde{\lambda}^*(t)$ are given in Equation (6) with N being replaced by Π/μ.

A detailed analysis of system (7) will be carried out in the following sections. Numerical simulations of the full system (4) suggest that all the behaviours identified for the reduced system (7) are also present in system (4). The results will be used to assess the effectiveness and implications of targeted antiviral prophylaxis strategy for disease control.

3. Reproduction numbers and equilibria

In this section, we consider the existence and stability of possible equilibria and determine how they depend on the reproduction numbers of the disease.

3.1. *Reproduction numbers and the disease-free equilibrium of system* (4)

The basic reproduction number (when $f = 0$) and the control reproductive number (when $f > 0$) for the full system (4) are

$$\mathcal{R}_0 = \frac{\beta k}{\eta + \mu} \quad \text{and} \quad \mathcal{R}_{cF} = \frac{(1-f)\beta k}{\eta + \mu} + \frac{f(1-c)\delta\beta k}{\theta\eta + \mu}, \tag{8}$$

respectively (the subscripts c for control and F for full system). Note that βk represents the average number of secondary infections produced by one untreated infectious person per unit time in a susceptible population, and $1/(\eta + \mu)$ represents the average infectious period of such an individual. Thus, $\mathcal{R}_0$ gives the average number of secondary infections produced by an untreated infectious individual during the entire infectious period in a susceptible population. Similarly, $(1 - f)\beta k/(\eta + \mu)$ and $f(1 - c)\delta\beta k/(\theta\eta + \mu)$ represent the average number of secondary infections generated by an untreated and treated (but transmission is not blocked) infectious individual, respectively. Thus, $\mathcal{R}_{cF}$ gives the reproductive number in the presence of treatment. Clearly, $\mathcal{R}_{cF} \leq \mathcal{R}_0$, and $\mathcal{R}_{cF} = \mathcal{R}_0$ if $f = 0$.

System (4) always has the disease-free equilibrium (DFE) $E_0 = (S^0, 0, 0, 0, 0)$, where $S^0 = \Pi/\mu$. The Jacobian matrix at E_0 has three negative eigenvalues $-\mu$, $-(\sigma + \mu)$, $-(\omega + \mu)$, and two other eigenvalues determined by the matrix

$$M = \begin{pmatrix} (1-f)\beta k - \eta - \mu & (1-f)\delta\beta k \\ f(1-c)\beta k & f(1-c)\delta\beta k - \theta\eta - \mu \end{pmatrix}.$$

It can be easily checked that both eigenvalues of M are negative if and only if $\mathcal{R}_{cF} < 1$. Thus, the following result holds.

THEOREM 3.1 *The DFE E_0 is locally asymptotically stable if $\mathcal{R}_{cF} < 1$ and unstable if $\mathcal{R}_{cF} > 1$.*

Theorem 3.1 implies that when $\mathcal{R}_{cF} < 1$ the infection level will go to zero if the initial population sizes are near E_0 (lie in the basin of attraction of E_0), which, however, does not guarantee that the disease will die out for arbitrary initial conditions. In fact, as shown in later sections, a stable endemic equilibrium is possible when the control reproductive number is less than one.

Assume that $\mathcal{R}_0 > 1$. The threshold condition $\mathcal{R}_{cF} < 1$ leads to the following critical value of treatment level

$$f_c = \frac{1 - (1/\mathcal{R}_0)}{1 - \delta(1-c)(\eta + \mu/\theta\eta + \mu)} > 0, \tag{9}$$

such that E_0 is l.a.s. if and only if $f > f_c$. We observe from Equation (9) that the possibility of reducing $\mathcal{R}_{cF}$ to be less than 1 by treatment f depends on several quantities, including the basic reproduction number $\mathcal{R}_0 = \beta/(\eta + \mu)$, the effect of treatment on the reduction of infectiousness (δ) and infectious period (θ), and the probability of transmission block (c). For example, if $\delta > 0$ and $c < 1$, then the quantity on the right-hand side of (9) is greater than 1 if

$$\mathcal{R}_0 > \frac{1}{\delta(1-c)(\eta + \mu/\theta\eta + \mu)}. \tag{10}$$

In this case, it is impossible to achieve $\mathcal{R}_{cF} < 1$ by treatment alone as $f \leq 1$.

3.2. *Endemic equilibria for reduced system* (7)

As the analysis about endemic equilibria of the full system (4) is very difficult due to the high dimension, the analytic results in this section will focus on the reduced system (7). Using $\delta = \theta = 1$ in Equation (8), we get the control reproductive number for Equation (7):

$$\mathcal{R}_c = \frac{(1 - fc)\beta k}{\eta + \mu} = (1 - fc)\mathcal{R}_0. \tag{11}$$

Note that, neither $\mathcal{R}_0$ nor $\mathcal{R}_c$ depend on γ (the reduction in susceptibility for individuals in the treated class P). However, as will be shown below, the existence and the number of endemic equilibria will depend on γ. In fact, as shown in the next result, $\gamma = 1/\mathcal{R}_0$ will provide a threshold value. In addition, another critical value,

$$\bar{\gamma} = 1 - fc. \tag{12}$$

also plays a key role in the analysis. Then the following relationships hold:

$$\gamma < (> \text{ or } =)\bar{\gamma} \quad \Longleftrightarrow \quad \gamma\mathcal{R}_0 < (> \text{ or } =)\mathcal{R}_c. \tag{13}$$

Let $E^*(x^*, y^*, z^*)$ denote an endemic equilibrium of system (7), i.e.

$$0 < x^*, y^*, z^* < 1.$$

Using the second and third equations in Equation (7) we have

$$\begin{aligned} y^* &= \frac{\mu + \omega}{\mu + \omega + \eta}\left[\left(\frac{\bar{\gamma}}{\gamma} - 1\right)x^* + \left(1 - \frac{1}{\gamma\mathcal{R}_0}\right)\right], \\ z^* &= \frac{\eta}{\mu + \omega}y^*. \end{aligned} \tag{14}$$

Using Equation (14) and the first equation of Equation (7), we have

$$F(x^*) = A(x^*)^2 + Bx^* + C = 0, \tag{15}$$

with

$$\begin{aligned} A &= [fk + (1 - f)(\mu + \eta)\mathcal{R}_0]\frac{\mu + \omega}{\mu + \omega + \eta}\left(1 - \frac{\bar{\gamma}}{\gamma}\right), \\ B &= 7 - \mu - [fk + (1 - f)(\mu + \eta)\mathcal{R}_0]\frac{\mu + \omega}{\mu + \omega + \eta}\left(1 - \frac{1}{\gamma\mathcal{R}_0}\right) \\ &\quad - \frac{\eta\omega}{\mu + \omega + \eta}\left(1 - \frac{\bar{\gamma}}{\gamma}\right) - \frac{\bar{\gamma}\sigma}{\gamma}, \\ C &= \mu + \frac{\mu + \omega}{\mu + \omega + \eta}\left(1 - \frac{1}{\gamma\mathcal{R}_0}\right) + \frac{\sigma}{\gamma\mathcal{R}_0}. \end{aligned} \tag{16}$$

If $A = 0$, i.e. $\gamma = \bar{\gamma}$, then Equation (15) has a unique solution $\hat{x}^* = -C/B$. Let

$$\hat{E}^*(\hat{x}^*, \hat{y}^*, \hat{z}^*) \tag{17}$$

denote the endemic equilibrium with

$$\hat{x}^* = -\frac{C}{B}, \quad \hat{y}^* = \frac{\mu + \omega}{\mu + \omega + \eta}\left(1 - \frac{1}{\mathcal{R}_c}\right), \quad \hat{z}^* = \frac{\eta}{\mu + \omega}\hat{y}^*. \tag{18}$$

If $A \neq 0$, i.e. $\gamma \neq \bar{\gamma}$, denote the two solutions of Equation (15) by

$$x_1^* = \frac{-B - \sqrt{B^2 - 4AC}}{2A}, \quad x_2^* = \frac{-B + \sqrt{B^2 - 4AC}}{2A}. \tag{19}$$

Let

$$E_i^*(x_i^*, y_i^*, z_i^*), \quad i = 1, 2, \tag{20}$$

denote the endemic equilibrium with x_i^* being given in Equation (19), and y_i^* and z_i^* given by Equation (14) for the corresponding $x_i^* (i = 1, 2)$. As mentioned above, in order for $\hat{E}^*$ or E_i^* to exist, we need to check that their components are between 0 and 1.

For ease of presenting the results for the existence of endemic equilibria, we need to introduce a threshold value of treatment f_m as defined below. Consider the case when $\mathcal{R}_0 > 1$ and $\mathcal{R}_c = (1 - fc)\mathcal{R}_0 < 1$. Let $f_m \in (0, 1)$ be the treatment fraction for which $\mathcal{R}_c = 1$, i.e.

$$(1 - f_m c)\mathcal{R}_0 = 1. \tag{21}$$

The following result on the existence of endemic equilibria for system (7) can be established.

THEOREM 3.2 *Let $\mathcal{R}_c$ be defined as in Equation* (11) *and let $\gamma > 0$.*

(a) *If $\mathcal{R}_c > 1$, then system* (7) *has a unique endemic equilibrium.*
(b) *If $\mathcal{R}_c \leq 1$, then system* (7) *has either no endemic equilibrium if γ is small, or possible multiple endemic equilibria if γ is large. More specifically,*
  (i) *if $\gamma \leq 1/\mathcal{R}_0$, then there is no endemic equilibrium;*
  (ii) *if $\gamma > 1/\mathcal{R}_0$, then system* (7) *may have 0, 1, or 2 endemic equilibria.*

Proof For the proof of part (a) we consider two cases, $\gamma > 1/\mathcal{R}_0$ and $\gamma \leq 1/\mathcal{R}_0$.

Case 1 $\gamma > 1/\mathcal{R}_0$. We first show that Equation (15) has a unique solution. Since $\gamma\mathcal{R}_0 > 1$, from Equation (16) we have $C > 0$. Thus,

$$F(0) = C > 0. \tag{22}$$

If we assume that $\sigma > \omega$ (i.e. the immunity gained from infection $(1/\omega)$ lasts longer than the immunity obtained from treatment $(1/\sigma)$, which is a reasonable assumption), then from $\mathcal{R}_c > 1$,

$$F(1) = \left[(fk + (1 - f)(\mu + \eta)\mathcal{R}_0)\frac{\mu + \omega}{\mu + \omega + \eta} + \frac{\eta(\sigma - \omega) + \sigma(\mu + \omega)}{\mu + \omega + \eta}\right]\frac{1 - \mathcal{R}_c}{\gamma\mathcal{R}_0} < 0. \tag{23}$$

Conditions (22) and (23) imply that the quadratic function $F(x)$ has a unique positive root x^* in $(0, 1)$. If $\gamma \neq \bar{\gamma}$ (either $\gamma > \bar{\gamma}$, in which case $A > 0$, or $\gamma < \bar{\gamma}$ in which case $A < 0$), then $x^* = x_1^*$ as given in Equation (19). If $\gamma = \bar{\gamma}$ then $A = 0$, in which case $x^* = \hat{x}^*$, which is given in Equation (18). It is clear from Equation (18) that $\hat{y}^* > 0$ and $\hat{z}^* > 0$. We now check the positivity of y^* and z^*.

If $\gamma > \bar{\gamma}$, from the y^* equation in (14) and $x^* = x_1^* < 1$ we have

$$\begin{aligned} y^* &> \frac{\mu + \omega}{\mu + \omega + \eta}\left[\left(\frac{\bar{\gamma}}{\gamma} - 1\right) + \left(1 - \frac{1}{\gamma\mathcal{R}_0}\right)\right] \\ &= \frac{\mu + \omega}{\mu + \omega + \eta}\frac{\mathcal{R}_c - 1}{\gamma\mathcal{R}_0} \\ &> 0. \end{aligned}$$

It is clear that $z^* > 0$ when $y^* > 0$. If $\gamma < \bar{\gamma}$, it is easy to see from Equation (14) that y^* and z^* are positive whenever $x^* > 0$. Therefore, there is a unique endemic equilibrium when $\mathcal{R}_c > 1$ and $\gamma > 1/\mathcal{R}_0$.

Case 2 $\gamma \le 1/\mathcal{R}_0$. From $\mathcal{R}_c = \bar{\gamma}\mathcal{R}_0 > 1$ and $\gamma\mathcal{R}_0 \le 1$, we know that $\gamma < \bar{\gamma}$ and $A < 0$. Let

$$\psi = \frac{1-\gamma\mathcal{R}_0}{\mathcal{R}_c - \gamma\mathcal{R}_0}. \tag{24}$$

Then $0 \le \psi < 1$, and it can be checked that

$$F(\psi) = \frac{(\sigma+\mu)(\mathcal{R}_c - 1)}{(\bar{\gamma}-\gamma)\mathcal{R}_0} > 0. \tag{25}$$

From (23), (25), and $A < 0$ we know that $F(x)$ has the unique root $x^* = x_1^*$ in $(\psi, 1)$. Using $x_1^* > \psi$, $\bar{\gamma} > \gamma$, and (14) we have

$$\begin{aligned} y_1^* &> \frac{\mu+\omega}{\mu+\omega+\eta}\left[\left(\frac{\bar{\gamma}}{\gamma}-1\right)\psi + \left(1-\frac{1}{\gamma\mathcal{R}_0}\right)\right] \\ &= \frac{(\mu+\omega)\psi}{(\mu+\omega+\eta)\gamma\mathcal{R}_0}[(\bar{\gamma}-\gamma)\mathcal{R}_0 + \gamma\mathcal{R}_0 - \mathcal{R}_c] \\ &= 0. \end{aligned}$$

It is clear that $z_1^* > 0$. Thus, E_1^* is the unique endemic equilibrium.

Proof of part (b). First we show part (i) that there is no endemic equilibrium when $\gamma \le 1/\mathcal{R}_0$.

If $\gamma \ge \bar{\gamma}$, then both terms in y^* given in (14) are either negative or zero if $x^* > 0$. Thus, E^* does not exist. If $\gamma < \bar{\gamma}$, from $\mathcal{R}_c \le 1$ we know that for $0 < x^* < 1$,

$$\begin{aligned} y^* &< \frac{\mu+\omega}{\mu+\omega+\eta}\left[\left(\frac{\bar{\gamma}}{\gamma}-1\right) + \left(1-\frac{1}{\gamma\mathcal{R}_0}\right)\right] \\ &= \frac{(\mu+\omega)(\mathcal{R}_c-1)}{(\mu+\omega+\eta)\gamma\mathcal{R}_0} \\ &\le 0. \end{aligned}$$

Thus, there is no endemic equilibrium.

Now we consider part (ii) and let $\gamma > 1/\mathcal{R}_0$. Consider two cases, $\mathcal{R}_c < 1$ and $\mathcal{R}_c = 1$.

Case 1 $\mathcal{R}_c < 1$. From $\mathcal{R}_c = \bar{\gamma}\mathcal{R}_0 < 1$ and $\gamma\mathcal{R}_0 > 1$, we know that $\gamma > \bar{\gamma}$. Notice that $A > 0$, $B < 0$, and $C > 0$. Notice also that

$$F(0) = C > 0 \quad \text{and} \quad F(\psi) > 0,$$

where $\psi \in (0, 1)$ is defined in Equation (24). Thus, $F(x)$ has the two roots $x_i^* \in (0, \psi)$ $(i = 1, 2)$ as given in Equation (19) if and only if

$$B^2 - 4AC \ge 0 \quad \text{and} \quad 0 < \frac{-B}{2A} < \psi, \tag{26}$$

one root $x_1^* = x_2^*$ if $B^2 - 4AC = 0$, and no root in $(0, \psi)$ otherwise.

Since $x_i^* < \psi (i = 1, 2)$ and $\bar{\gamma} < \gamma$, from Equation (14) we have

$$\begin{aligned} y_i^* &> \frac{\mu + \omega}{\mu + \omega + \eta} \left[\left(\frac{\bar{\gamma}}{\gamma} - 1 \right) \psi + \left(1 - \frac{1}{\gamma \mathcal{R}_0} \right) \right] \\ &= \frac{(\mu + \omega)\psi}{(\mu + \omega + \eta)\gamma \mathcal{R}_0} \left[(\bar{\gamma} - \gamma)\mathcal{R}_0 + \gamma \mathcal{R}_0 - \mathcal{R}_c \right] \\ &= 0, \quad i = 1, 2. \end{aligned}$$

It follows that $z_i^* > 0 (i = 1, 2)$. Thus, both E_1^* and E_2^* exist if $\gamma > 1/\mathcal{R}_0$ and conditions in Equation (26) hold.

Clearly, $x_1^* = x_2^*$ if $B^2 - 4AC = 0$; and thus, $F(x)$ has a unique root in $(0, \psi)$, which corresponds to the unique endemic equilibrium E_1^*. It is also easy to see that if $B^2 - 4AC < 0$ or $-B/2A > \psi$, then $F(x)$ has no root in $(0, \psi)$.

Since $\psi < 1$, it remains to show that there is no endemic equilibrium E^* with $x^* \in [\psi, 1)$. Note that, for any $x^* < \psi$, from Equation (14) and using a similar estimate as above, we can show that $y^* < 0$. Hence, there is no E^* with $x^* \in [\psi, 1)$.

Case 2 $\mathcal{R}_c = 1$. Since $\gamma \mathcal{R}_0 > 1$, we have $\gamma > \bar{\gamma}$. In this case, $A > 0$, $B < 0$, and $C > 0$. Note that $F(0) = C > 0$ and $F(1) = 0$. Thus, the equation $F(x) = 0$ has a unique root x^* which lies in $(0, 1)$ if and only if conditions in Equation (26), in which case $x^* = x_1^*$.

The proof of Theorem 3.2 is completed. ■

It will be useful to rewrite the conditions in Equation (26) in terms of model parameters, e.g. the treatment fraction f and the reinfection coefficient γ. It is important to notice that $\mathcal{R}_0$ and $\mathcal{R}_c$ do not depend on γ. Notice also that $\mathcal{R}_c < 1$ requires $f > f_m$ (f_m is given in Equation (21). It is not easy to obtain such expressions from Equation (26) analytically. Nonetheless, using parameter values in the next section (Table 2), our numerical calculations suggest that for each fixed $\gamma > 1/\mathcal{R}_0$, the condition $B^2 - 4AC = 0$ determines a threshold value $f^* = f^*(\gamma)$ such that $f_m \leq f^*(\gamma) \leq 1$ and that

$$f < (= \text{or} >) f^*(\gamma) \quad \Longleftrightarrow \quad B^2 - 4AC > (= \text{or} <) 0 \tag{27}$$

(Figure 2). Note that $\mathcal{R}_c = (1 - fc)\mathcal{R}_0$. Let

$$\mathcal{R}_c^*(\gamma) = (1 - f^*(\gamma)c)\mathcal{R}_0,$$

then $\mathcal{R}_c^*(\gamma) > (= \text{or} <) 1$ if $f < (= \text{or} >) f_m$, and the conditions in Equation (27) can be rewritten as

$$\mathcal{R}_c > (= \text{or} <) \mathcal{R}_c^* \quad \Longleftrightarrow \quad B^2 - 4AC > (= \text{or} <) 0. \tag{28}$$

Table 2. Parameter values used in simulations (values are appropriate to influenza).

Parameter	Estimated value	Unit
$\frac{\Pi}{\mu}$	10,000	–
μ	0.00005	Days^{-1}
ω	0.006	Days^{-1}
σ	0.05	Days^{-1}
β	0.01417	–
k	30	–
c	0.85	–
η	0.1667	Days^{-1}

In addition, for the set of parameter values used, the condition $B^2 - 4AC > 0$ implies $-B/(2A) < \psi$. It follows that, when $\mathcal{R}_c < 1$, an endemic equilibrium exists if and only if $\mathcal{R}_c \geq \mathcal{R}_c^*(\gamma)$.

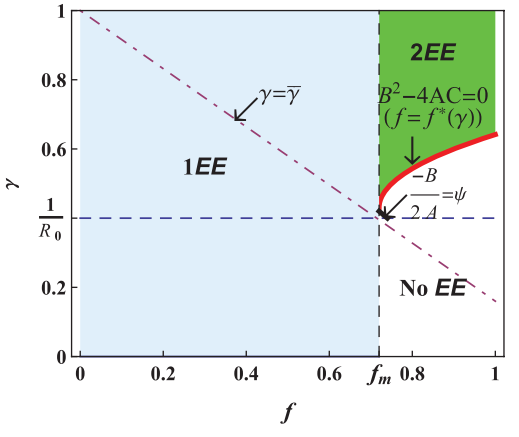

Figure 2. A bifurcation diagram in the (f, γ)-plane for system (7). Other parameter values are given in Table 2. No EE denotes no endemic equilibrium, 1EE stands for only one endemic equilibrium, 2EE stands for two endemic equilibria. It shows that for $\mathcal{R}_c > 1$ (on the left of $\mathcal{R}_c = 1$, which is equivalent to $f < f_m$), there is a unique endemic equilibrium. For $\mathcal{R}_c < 1$ (which corresponds to $f > f_m$), if $\gamma \leq 1/\mathcal{R}_0$ then there is no endemic equilibrium. However, when $\gamma > 1/\mathcal{R}_0$, there is a curve $f^*(\gamma)$ (which corresponds to the curve determined by $B^2 - 4AC = 0$) such that the system has two endemic equilibria if $f < f^*$, one endemic equilibrium if $f = f^*$, and no endemic equilibrium if $f > f^*$.

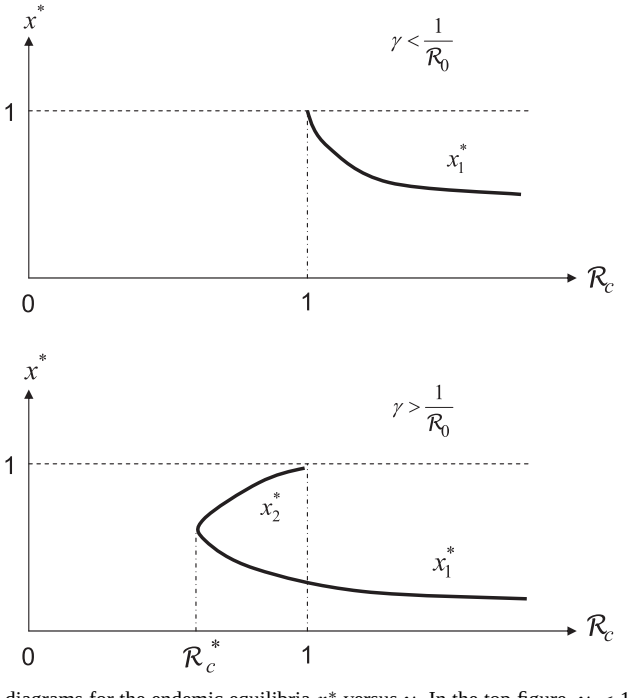

Figure 3. Bifurcation diagrams for the endemic equilibria x_i^* versus γ. In the top figure, $\gamma < 1/\mathcal{R}_0$ and it shows that there is no endemic equilibrium for $\mathcal{R}_c < 1$. In the bottom figure, $\gamma > 1/\mathcal{R}_0$ and shows that there is a unique endemic equilibrium x_1^* for $\mathcal{R}_c > 1$. For $\mathcal{R}_c \leq 1$, there are two endemic equilibria (x_1^* and x_2^*) for $\mathcal{R}_c \in (\mathcal{R}_c^*, 1)$, one equilibrium ($x_1^* = x_2^*$) for $\mathcal{R}_c = \mathcal{R}_c^*$, and no endemic equilibrium for $\mathcal{R}_c < \mathcal{R}_c^*$. The value of $\mathcal{R}_c^*$ depends on γ.

The two endemic equilibria are given by E_1^* and E_2^*, and $E_1^* = E_2^*$ if $\mathcal{R}_c = \mathcal{R}_c^*(\gamma)$. There is no endemic equilibrium if $\mathcal{R}_c < \mathcal{R}_c^*(\gamma)$.

Results stated in Theorem 3.2 are also summarized in the bifurcation diagrams shown in Figure 3. We observe that there is a backward bifurcation for $\gamma > 1/\mathcal{R}_0$, i.e. endemic equilibria exist when the reproductive number $\mathcal{R}_c$ is less than unity. Moreover, when $\mathcal{R}_c < 1$, stable periodic solutions also exist for (f, γ) in a certain region.

4. Stability and bifurcation

In this section, we mainly apply the local bifurcation theory to explore the dynamics of system (7). We shall show that system (7) may undergo Hopf bifurcation. In order to show that system (7) may undergo Hopf bifurcation, we first investigate the local stability of the endemic equilibria for system (7). Let $E^*(x^*, y^*, z^*)$ be an endemic equilibrium of system (7). Linearizing around the endemic equilibrium E^*, we obtain the matrix

$$J(E^*) = \begin{pmatrix} -\mu - (f+\beta - f\beta)ky^* - \sigma & -(f+\beta-f\beta)kx^* - \sigma & \omega - \sigma \\ (1 - fc - \gamma)\beta ky^* & -\gamma\beta ky^* & -\gamma\beta ky^* \\ 0 & \eta & -(\mu+\omega) \end{pmatrix}. \quad (29)$$

After extensive algebraic calculations, its characteristic equation is given by

$$\lambda^3 + A_1(E^*)\lambda^2 + A_2(E^*)\lambda + A_3(E^*) = 0, \quad (30)$$

where

$$\begin{aligned} A_1(E^*) &= 2\mu + \sigma + \omega + (f + \gamma\beta + \beta - f\beta)ky^* > 0; \\ A_2(E^*) &= (\mu + \sigma + (f+\beta-f\beta)ky^*)(\mu + \omega + \gamma\beta ky^*) + \gamma\beta ky^*(\mu + \omega + \eta) \\ &\quad - (\sigma + (f+\beta-f\beta)kx^*)(fc + \gamma - 1)\beta ky^*; \\ A_3(E^*) &= -(\mu+\omega+\eta)\gamma\beta ky^* \frac{2(fc+\gamma-1)(\mu+\omega)(f+\beta-f\beta)k}{\gamma(\mu+\omega+\eta)}x^* - \mu - \sigma \\ &\quad - \frac{(f+\beta-f\beta)k(\mu+\omega)(\gamma\mathcal{R}_0 - 1)}{\gamma\mathcal{R}_0(\mu+\omega+\eta)} + \frac{(fc+\gamma-1)(\sigma(\mu+\omega+\eta) - \eta\omega)}{\gamma(\mu+\omega+\eta)}\Bigg) \\ &= -(\mu+\omega+\eta)\gamma\beta ky^*(2Ax^* + B), \end{aligned}$$

where A and B are given in Equation (16).

For the sake of the convenience, we define

$$H(E^*) = A_1(E^*)A_2(E^*) - A_3(E^*),$$

and let $W^u(E^*)$ be the unstable manifold of E^*, $W^s(E^*)$ be its stable manifold and $W^c(E^*)$ be its centre manifold. Then we have

THEOREM 4.1 *Let E_1^* and E_2^* be the endemic equilibria of system* (7) *as defined before.*

(1) *Assume that $\mathcal{R}_c > 1$. Then,*
   (a) *if $H(E_1^*) > 0$, then* $\dim W^s(E_1^*) = 3$, *i.e. the unique positive equilibrium is locally asymptotically stable;*

(b) *if* $H(E_1^*) < 0$, *then* $\dim W^s(E_1^*) = 1$, $\dim W^u(E_1^*) = 2$, *i.e. the unique endemic equilibrium* E_1^* *is unstable; and*
(c) *if* $H(E_1^*) = 0$ *then* $\dim W^c(E_1^*) = 2$ *and* $\dim W^s(E_1^*) = 1$.

(2) *Assume that* $\mathcal{R}_c < 1$ *and that both* E_1^* *and* E_2^* *exist. Then,*
(a) $\dim W^s(E_2^*) = 2$, $W^u(E_2^*) = 1$, *i.e. the endemic equilibrium* E_2^* *is unstable;*
(b) *if* $H(E_1^*) > 0$, *then* $\dim W^s(E_1^*) = 3$, *i.e.* E_1^* *is locally asymptotically stable;*
(c) *if* $H(E_1^*) < 0$, *then* $\dim W^s(E_1^*) = 1$, $\dim W^u(E_1^*) = 2$, *i.e.* E_1^* *is unstable; and*
(d) *if* $H(E_1^*) = 0$, *then* $\dim W^c(E_1^*) = 2$, $\dim W^s(E_1^*) = 1$.

Proof Let $\lambda_1, \lambda_2, \lambda_3$ be the roots of Equation (30) and, without the loss of generality, assume that $\Re\lambda_1 \le \Re\lambda_2 \le \Re\lambda_3$.

Assume that $\mathcal{R}_c > 1$, then Theorem 3.2 indicates that system (7) has a unique endemic equilibrium $E_1^*(x_1^*, y_1^*, z_1^*)$, where x_1^* is a root of Equation (15) and satisfies $F'(x_1^*) = 2Ax_1^* + B < 0$. It follows from the relations between the roots and the polynomial coefficients that

$$\begin{aligned}\lambda_1 + \lambda_2 + \lambda_3 &= -A_1(E_1^*) < 0,\\ \lambda_1\lambda_2\lambda_3 &= -A_3(E_1^*)\\ &= (\mu + \omega + \eta)\gamma\beta k y^*(2Ax_1^* + B) < 0.\end{aligned}$$

This means that either $\Re\lambda_i < 0$ for $j = 1, 2, 3$ or $\Re\lambda_1 < 0 \le \Re\lambda_2 \le \Re\lambda_3$. If $H(E_1^*) > 0$, then the Routh–Hurwitz conditions indicate that $\Re\lambda_i < 0$ for $j = 1, 2, 3$. By the Hartman–Grobman Theorem, we have $\dim W^s(E_1^*) = 3$, i.e. the unique positive equilibrium is locally asymptotically stable. If $H(E_1^*) = 0$, then we have $A_2(E_1^*) < 0$ since $A_1(E_1^*) > 0$, $A_3(E_1^*) < 0$. It is easy to verify that $\pm\sqrt{-A_2(E_1^*)}i$ are two roots of Equation (30). This, together with the fact $\Re\lambda_1 < 0$, implies that $\Re\lambda_1 < 0$, $\lambda_2 = -\sqrt{-A_2(E_1^*)}i$, $\lambda_2 = +\sqrt{-A_2(E_1^*)}i$. It also follows from Hartman–Grobman Theorem that $\dim W^s(E_1^*) = 1$, $\dim W^c(E_1^*) = 2$. If $H(E_1^*) < 0$, then the Routh–Hurwitz conditions indicate that $\Re\lambda_1 < 0$, $\Re\lambda_2 > 0$, $\Re\lambda_3 > 0$. By the Hartman–Grobman theorem, we have $\dim W^s(E_1^*) = 1$, $\dim W^u(E_1^*) = 2$, i.e. the unique positive equilibrium E_1^* is unstable. The proof of part 1 is finished.

Assume $\mathcal{R}_c < 1$ and system (7) has two endemic equilibria, $E_1^*(x_1^*, y_1^*, z_1^*)$ and $E_2^*(x_2^*, y_2^*, z_2^*)$. From the proof of Theorem 3.2, we have that x_1^* and x_2^* are the roots of Equation (15) and

$$\begin{aligned}F'(x_1^*) &= 2Ax_1^* + B < 0,\\ F'(x_2^*) &= 2Ax_2^* + B > 0.\end{aligned}$$

The stability results for E_1^* can be obtained using the same argument as in the proof of part 1 above, which will be omitted here.

Now we consider the local stability of E_2^*. It follows from the relations between the roots and the polynomial coefficients that

$$\begin{aligned}\lambda_1 + \lambda_2 + \lambda_3 &= -A_1(E_2^*) < 0,\\ \lambda_1\lambda_2\lambda_3 &= -A_3(E_2^*)\\ &= (\mu + \omega + \eta)\gamma\beta k y^*(2Ax_2^* + B) > 0.\end{aligned}$$

This implies that $\Re\lambda_1 < 0$, $\Re\lambda_2 < 0$, $\Re\lambda_3 > 0$. It follows from the Hartman–Grobman Theorem that $\dim W^s(E_2^*) = 2$, $\dim W^u(E_2^*) = 1$, i.e. the endemic equilibrium E_2^* is unstable. This completes the proof of Theorem 4.1. ■

We remark that in Theorem 4.1, for the case $\mathcal{R}_c < 1$, the merging of E_1^* and E_2^* constitutes a limit point (LP) (saddle-node) bifurcation. While Hopf bifurcation has been shown to occur

along the E_1^* branch of solutions, it is also possible that a codimension-2 bifurcation may occur when the Hopf and LP bifurcations merge, leading to a Bogdanov–Takens bifurcation. This kind of analysis has been done for an SIRS model in [1, Figures 5.4 and 5.7]. Theorem 4.1 also shows that dim $W^c(E_1^*) = 2$ when $H(E_1^*) = 0$. It then follows that any exchange stability of E_1^* will undergo Hopf bifurcation. As was done in the existence results, we choose γ (reduction in susceptibility for individuals in the treated class P) to be the bifurcation parameter. For simplicity, we introduce new notions. Let $E_1^*(x_1^*(\gamma), y_1^*(\gamma), z_1^*(\gamma))$ be the corresponding endemic equilibrium of system (7), and let

$$\lambda^3 + A_1^*(\gamma)\lambda^2 + A_2^*(\gamma)\lambda + A_3^*(\gamma) = 0$$

be the characteristic equation of the variational system associated with Equation (7) about E_1^*. Set

$$H(\gamma) = A_1^*(\gamma)A_2^*(\gamma) - A_3^*(\gamma).$$

We can establish the following Theorem 4.2.

THEOREM 4.2 *Assume that system (7) has either a unique positive equilibrium, which is given by $E_1^*(x_1^*(\gamma), y_1^*(\gamma), z_1^*(\gamma))$, or two positive equilibria, which are given by $E_1^*(x_1^*(\gamma), y_1^*(\gamma), z_1^*(\gamma))$ and $E_2^*(x_2^*(\gamma), y_2^*(\gamma), z_2^*(\gamma))$. If there exists $\gamma = \gamma_c$ such that*

$$H(\gamma_c) = 0, \quad H'(\gamma_c) < 0 (H'(\gamma_c) > 0), \tag{31}$$

then the endemic equilibrium $E_1^*(x_1^*(\gamma), y_1^*(\gamma), z_1^*(\gamma))$ is locally stable (unstable) if $\gamma < \gamma_c$ and $\gamma_c - \gamma \ll 1$, while it is unstable (locally stable) for $\gamma > \gamma_c$ and $\gamma - \gamma_c \ll 1$. Moreover, a Hopf bifurcation occurs at $\gamma = \gamma_c$ and stable periodic solutions exist for $\gamma > \gamma_c$ and $\gamma_c - \gamma \ll 1$. Although it is not easy to derive an analytic expression for γ_c, numerical simulations showed that there exist two critical points γ_{ci}, $i = 1, 2$, for parameter values in Table 2.

Proof We only prove the conclusion outside the brackets. The conclusion inside the brackets can be proved in a similar way. The fact that $H'(\gamma_c) < 0$ indicates that $H(\gamma)$ is a monotonic decreasing function in the neighbourhood of $\gamma = \gamma_c$. This, together with $H(\gamma_c) = 0$, implies that $H(\gamma) > 0$ for $\gamma < \gamma_c$ and $\gamma_c - \gamma \ll 1$. Thus, by Theorem 4.1, we have $\Re\lambda_i < 0$ for $i = 1, 2, 3$; and thus, the endemic equilibrium $E_1^*(x_1^*(\gamma), y_1^*(\gamma), z_1^*(\gamma))$ is locally stable. The fact that $H(\gamma)$ is a monotonic decreasing function in the neighbourhood, $\gamma = \gamma_c$ also implies that $H(\gamma) < 0$ for $\gamma > \gamma_c$ and $\gamma - \gamma_c \ll 1$. Then, it follows from Theorem 4.1 that we have $\Re\lambda_2(\gamma) < 0$ and $\Re\lambda_3(\gamma) < 0$, which implies that the endemic equilibrium $E_1^*(x_1^*(\gamma), y_1^*(\gamma), z_1^*(\gamma))$ is unstable. According to the result in [17], the conditions $H(\gamma_c) = 0$ and $H'(\gamma_c) < 0$ imply the occurrence of a simple Hopf bifurcation at $\gamma = \gamma_c$.

The identification of an analytic expression for γ_c and the examination of the conditions $H(\gamma_c) = 0$ and $H'(\gamma_c) < 0$ are very difficult. Nevertheless, these can be done numerically (see Figures 4–7 in the next section). For the set of parameter values listed in Table 2, two critical points, γ_{c1} and γ_{c2}, exist for both the case $\mathcal{R}_c > 1$ (Figure 4) and the case $\mathcal{R}_c < 1$ (Figure 6).

This completes the proof of Theorem 4.2. ■

We remark that, although the existence and stability analysis in this section is carried out for the reduced system (7), our numerical simulations show that similar dynamical behaviours are also present in the full system (4) (i.e. for the case when $\delta < 1$ and/or $\theta < 1$). More details about numerical studies are provided in the next section.

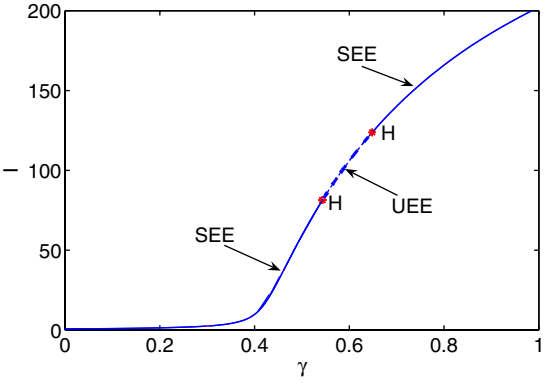

Figure 4. Plot of the unique endemic equilibrium (the component I of infectious individuals, where $I = x \times (\Pi/\mu) = x \cdot 10^4$) versus γ for the case $\mathcal{R}_c > 1$ for system (7). The value of f is chosen to be $f = 0.7 < f_m$. All other parameter values are listed in Table 2. SEE stands for the stable endemic equilibrium (solid curve) and UEE stands for the unstable endemic equilibrium (dash curve). H denotes Hopf bifurcation, and it shows that two Hopf bifurcations occur at $\gamma_{c1} = 0.543$ and $\gamma_{c2} = 0.648$.

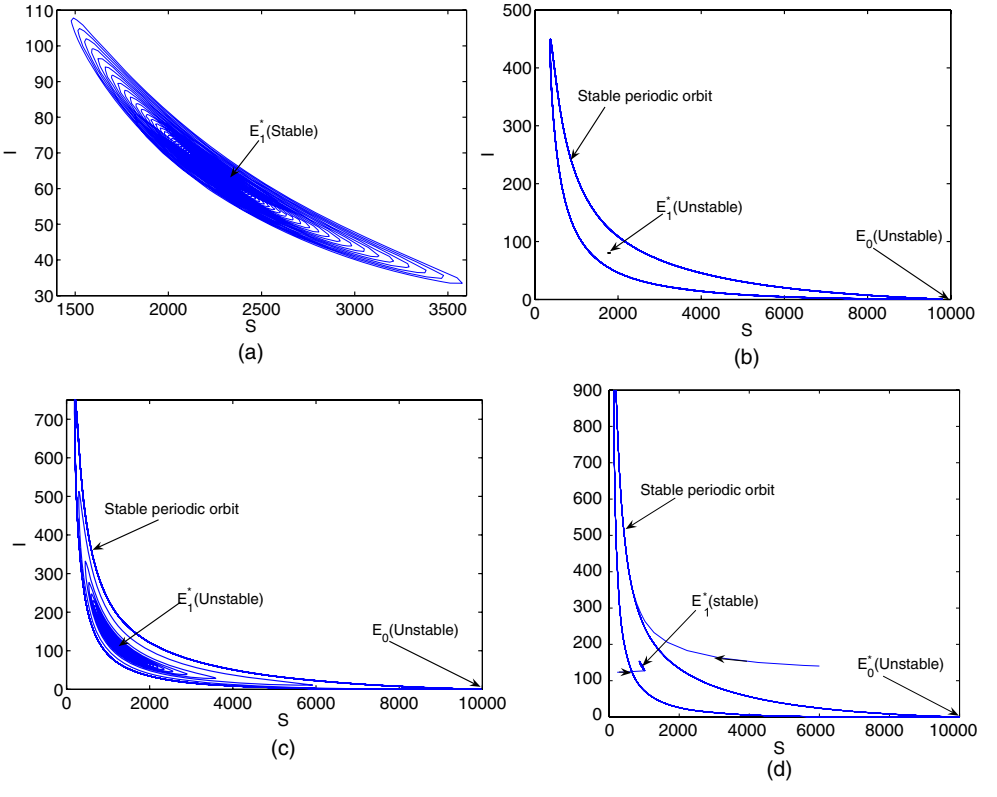

Figure 5. Numerical simulations (phase portraits) of system (7) for various γ values chosen according to the bifurcation diagram in Figure 4 ($\mathcal{R}_c > 1$). Other parameter values are the same as in Figure 4. In (a), $\gamma = 0.51$, which is to the left of the first Hopf bifurcation point $\gamma_{c1} = 0.543$. It shows that the unique endemic equilibrium E_1^* is stable. In (b), $\gamma = 0.56$, which is slightly to the right of the first Hopf bifurcation point $\gamma_{c1} = 0.543$. The trajectory shown is a stable period solution. In (c), $\gamma = 0.63$, which is slightly to the left of the second Hopf bifurcation point $\gamma_{c2} = 0.648$. It shows that solutions converge to a stable periodic solution. In (d), $\gamma = 0.7$, which is to the right of γ_{c2}. It shows that solutions starting near the endemic equilibrium E_1^* will converge to E_1^* (see the short curve near E_1^*), while other solutions starting far away from E_1^* converge to a stable periodic solutions (the larger orbit).

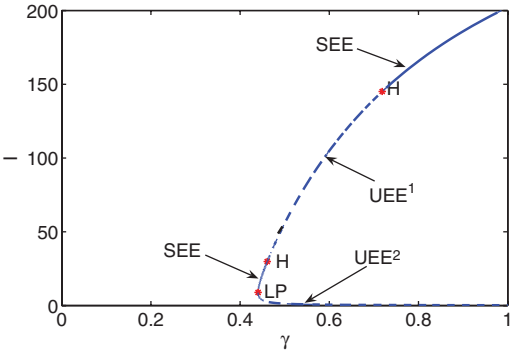

Figure 6. Similar to Figure 4 except that $\mathcal{R}_c < 1$. The value of f is chosen to be $f = 0.72 > f_m$. All other parameter values are listed in Table 2. It shows that there are two branches of endemic equilibria, separated by an LP. The top branch corresponds to E_1^* and the bottom one corresponds to E_2^*. SEE stands for the stable endemic equilibrium (solid curve) and UEE^i stands for unstable endemic equilibrium (dash curve) for E_i^*, $i = 1, 2$. H denotes Hopf bifurcation, and it shows that along the top branches two Hopf bifurcations occur at $\gamma_{c1} = 0.460$ and $\gamma_{c2} = 0.719$.

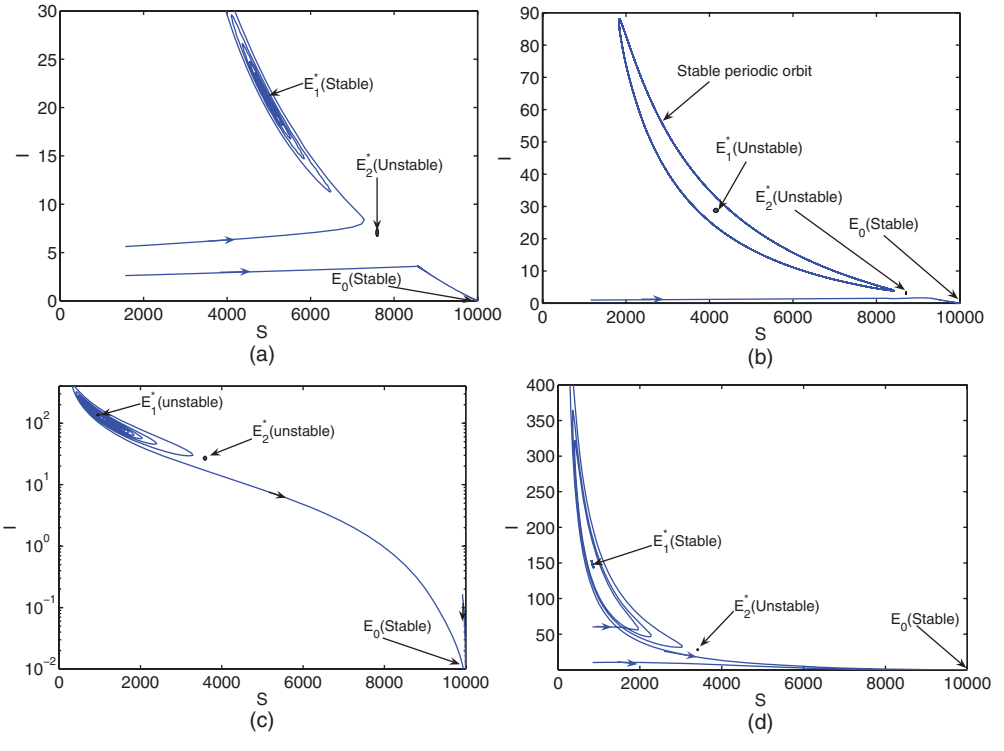

Figure 7. Similar to Figure 5 except that various γ values are chosen according to the bifurcation diagram in Figure 6, in which $f = 0.72$ and $\mathcal{R}_c < 1$. All other parameters have the same values. In (a), $\gamma = 0.45$, which is to the left of the first Hopf bifurcation point $\gamma_{c1} = 0.46$. It shows that depending on initial conditions, solutions will converge to either endemic equilibrium E_1^* or the DFE. In (b), $\gamma = 0.47$, which is slightly to the right of the first Hopf bifurcation point $\gamma_{c1} = 0.460$. The larger (closed) orbit shown is a stable period solution. We observe that, depending on initial conditions, solutions may also converge to the DFE. In (c), $\gamma = 0.69$, which is not close to either γ_{c1} or γ_{c2}. In this case, although both endemic equilibria are unstable, there is no stable periodic solution. It shows that all solutions converge to the DFE. In (d), $\gamma = 0.73$, which is to the right of γ_{c2}. It shows a similar scenario to (a), i.e. solutions converge either to E_1^* or the DFE, depending on the initial condition.

5. Numerical simulations

In this section, we present numerical results from simulations for both the reduce system (7) and the full system (4). These simulations not only confirm the analytical results described in the last section, but also extend these results to more general case and illustrate more complex behaviours of the model system including an homoclinic orbit and bistability scenarios.

The parameter values used in the simulations are chosen for illustration purposes. We choose

$$\Pi = 0.5,\ \mu = 0.00005,\ \omega = 0.006,\ \sigma = 0.05,\ \beta = 0.01417,\ k = 30,\ c = 0.85,\ \eta = 0.1667.$$

In this case, we have $\mathcal{R}_0 = 2.54$. All parameter values used in simulations are summarized in Table 2. As is shown in the analysis in the last section, the parameters for treatment (f) and for reduction in susceptibility by prophylaxis (γ) will vary in the numerical studies as well.

Using the parameter values listed in Table 2, we can generate a bifurcation diagram in the (f, γ)-plane as shown in Figure 2. We observe that the number of endemic equilibria of system (7) is determined by the two curves, $\gamma^*(f)$ (along which $B^2 - 4AC = 0$) and $f = f_m$ (along which $\mathcal{R}_c = 1$). For example, in the region $f < f_m$ (in which $\mathcal{R}_c > 1$), there is a unique endemic equilibrium. In the region $f > f_m$ (in which $\mathcal{R}_c < 1$), the number of endemic equilibrium is two if $\gamma > \gamma^*(f)$, one if $\gamma = \gamma^*(f)$, or zero if $\gamma < \gamma^*(f)$.

We present next simulation results for both the case $\mathcal{R}_c > 1$ (Figures 4 and 5) and the case $\mathcal{R}_c < 1$ (Figures 6 and 7).

Figure 4 shows a bifurcation diagram for the system (7), with γ as the bifurcation parameter and a fixed value of $f = 0.7 < f_m$ (for which $\mathcal{R}_c > 1$). In this case, analytical results show that there is a unique endemic equilibrium given by E_1^* for all γ. This is illustrated in Figure 4 by the curve I_1^* (the number of infectious individuals at the equilibrium) that varies with γ. It also identifies two Hopf bifurcation points at γ_{c1} and γ_{c2}, and indicates that E_1^* is stable for $\gamma < \gamma_{c1}$ and $\gamma > \gamma_{c2}$, and unstable if $\gamma_{c1} < \gamma < \gamma_{c2}$. More specifically, numerically solving the equation $H(\gamma) = 0$ (see Equation 31) gives that $\gamma_{c1} = 0.543$ and $\gamma_{c2} = 0.648$, and further calculations yield that $H'(\gamma_{c1}) = -0.00036 < 0$ and $H'(\gamma_{c2}) = 0.00043 > 0$. Denote E_1^* by $E_1^*(\gamma)$. By evaluating the first Lyapunov coefficient ($\mathfrak{L}_1(\gamma)$) [15] of system (7) at $E_1^*(\gamma_{ci})$), $i = 1, 2$, we find that

$$\mathfrak{L}_1(\gamma_c^1) \approx -9.4 \times 10^{-7} < 0 \quad \text{and} \quad \mathfrak{L}_1(\gamma_c^2) \approx 1.28 \times 10^{-9} > 0.$$

Hence, system (7) undergos a supercritical Hopf bifurcation at $\gamma = \gamma_{c1}$ and a subcritical Hopf bifurcation at $\gamma = \gamma_{c2}$, where supercritical Hopf bifurcation implies the appearance of a stable limit cycle when γ passes through γ_{c1} while subcritical Hopf bifurcation implies the appearance of an unstable limit cycle when γ passes through γ_{c2}. These behaviours are illustrated in Figure 5.

In Figure 5, where $\mathcal{R}_c > 1$, various γ values are chosen according to the bifurcation diagram in Figure 4. These values are $\gamma = 0.51, 0.56, 0.63, 0.70$ in Figures 5(a)–(d), respectively. All other parameter values are the same as in Figure 2. In Figure 5(a), $\gamma = 0.51 < \gamma_{c1}$, the unique positive equilibrium $E_1^*(S_1^*, I_1^*, R_1^*) = (2243.578, 64.6746, 1782.03)$ is shown to be locally asymptotically stable. In Figure 5(b), $\gamma = 0.56$ is slightly bigger than γ_{c1}, and the trajectory shown is a stable periodic solution, as in this case the unique endemic equilibrium $E_1^* = (1627.89, 89.12, 2455.65)$ is unstable. For $\gamma = 0.63$, which is lightly less than γ_{c2}, Figures 5(c) shows that the unique endemic equilibrium $E_1^*(1182.21, 117.373, 3234.05)$ is unstable and the solutions converge to a stable periodic solution.

In Figure 5(d), $\gamma = 0.70 > \gamma_{c2}$. The behaviours of the solutions are very different from those in Figure 5(a)–(c). The unique endemic equilibrium is $E_1^*(934.59, 140.17, 3862.24)$, which is locally asymptotically stable. Simulations indicate that, while solutions starting from near E_1^* will converge to E_1^*, other solutions with initial conditions not close to E_1^* will converge to a stable periodic solution (Figure 5(d)). Hence, besides the unstable periodic solution bifurcated

from the equilibrium E_1^*, there is another stable periodic solution, indicating that the existence of two periodic orbits is possible.

Figure 6 is a bifurcation diagram similar to Figure 4 but is for the case of $\mathcal{R}_c < 1$. The value of f is chosen to be $f = 0.72 > f_m$. All other parameter values are the same as those in Figure 5. In this case, an endemic equilibrium exists only for $\gamma > \gamma_c^{\mathrm{LP}} = 0.44$ (here LP denote limit point). Simulations suggest that when $\gamma < \gamma_c^{\mathrm{LP}}$, the DFE is globally asymptotically stable. For $\gamma > \gamma_c^{\mathrm{LP}}$, there are two branches of endemic equilibria, with the top and bottom branches corresponding to E_1^* and E_2^*, respectively. Denote $E_i^* = E_i^*(\gamma)$, $i = 1, 2$. $E_2^*(\gamma)$ is unstable for all γ. For $E_1^*(\gamma)$, Numerical calculations show that there are two Hopf bifurcations at $\gamma_{c1} = 0.460$ and $\gamma_{c2} = 0.719$, with $H'(\gamma_{c1}) = -0.0006 < 1$ and $H'(\gamma_{c2}) = 0.001 > 0$. Thus, from Theorem 4.2, $E_1^*(\gamma)$ is stable for $\gamma_c^{\mathrm{LP}} < \gamma < \gamma_{c1}$ and $\gamma > \gamma_{c2}$, and unstable for $\gamma_{c1} < \gamma < \gamma_{c2}$. Moreover, dim $W^s(E_2^*) = 2$ and dim $W^u(E_2^*) = 1$. Evaluating the first Lyapunov coefficient of system (7) at $E_1^*(\gamma_{ci})$), $i = 1, 2$, we have

$$\mathfrak{L}(\gamma_{c1}) = -1.93 \times 10^{-11} < 0 \quad \text{and} \quad \mathfrak{L}(\gamma_{c2}) = 1.94 \times 10^{-9} > 0.$$

It follows that system (7) undergos a supercritical Hopf bifurcation at γ_{c1} and a subcritical Hopf bifurcation at $\gamma = \gamma_{c2}$.

Figure 7 is similar to Figure 5 except that it shows phase portraits for various γ values chosen according to the bifurcation diagram in Figure 6. The parameter values used in Figures 7(a)–(d) are $\gamma = 0.45,\ 0.47,\ 0.69,\ 0.73$, respectively. All other parameter values are the same as in Figure 6. In Figure 7(a), the value $\gamma = 0.45$ satisfies $\gamma_c^{\mathrm{LP}} < \gamma < \gamma_{c1}$, it shows that there are two positive equilibria, $E_1^*(S_1^*, I_1^*, R_1^*) = (4946.19, 21.07, 580.55)$ and $E_2^*(S_2^*, I_2^*, R_2^*) = (8561.20, 3.63, 99.93)$. We observe that, depending on initial conditions, solutions may either converge to E_1^* or converge to the DFE. In Figure 7(b), $\gamma = 0.47$ is slightly bigger than γ_{c1}. We observe a stable periodic solutions. Again, depending on initial conditions, solutions may either converge to the periodic solution or converge to the DFE. Figure 7(c) illustrates solution behaviours that are very different from those shown in Figure 1 for the case of $\mathcal{R}_c > 1$. This is for $\gamma = 0.69$, which is not close to either γ_{c1} or γ_{c2}. It shows that solutions starting near E_1^*, instead of converging to the periodic solution bifurcated from E_1^*, are converging to the DFE. This may indicate the possibility that a homoclinic bifurcation exists (Figure 8). Figure 7(d) is for $\gamma = 0.73 > \gamma_{c2}$. It shows that solutions may converge to either the stable endemic equilibrium E_1^* or the stable DFE, depending on initial conditions.

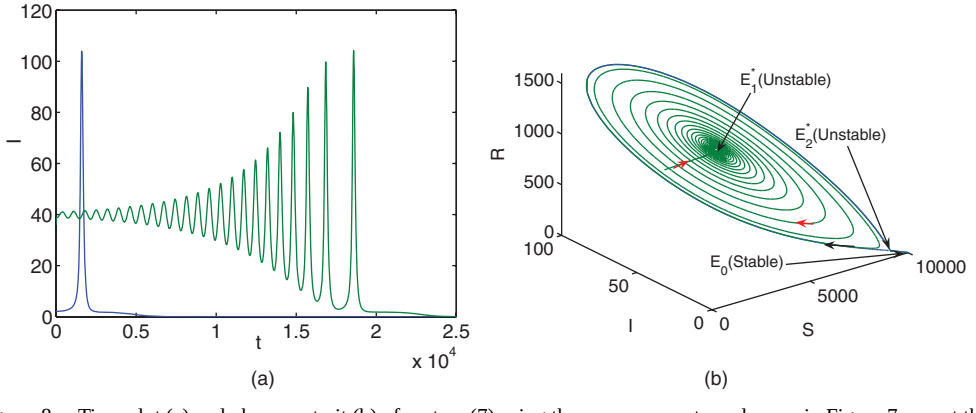

Figure 8. Time plot (a) and phase portrait (b) of system (7) using the same parameter values as in Figure 7 except that $\gamma = 0.475$, which is between γ_{c1} and γ_{c2}. It shows that solutions will converge to the DFE, regardless of initial conditions. It also illustrates the possibility that a homoclinic orbit exists (as a consequence that the stable periodic orbit around E_1^* merges with the endemic equilibrium E_2^*).

Figure 8 illustrate the possible existence of a homoclinic orbit. The same set of parameter values as in Figure 7 is used except that $\gamma = 0.475$. Figure 8(a) is a time plot of the number of infectious individuals $I(t)$. It shows two solutions, one with initial value near zero and the other one with initial condition near E_1^*. Both solutions are going to the DFE. Figure 8(b) plot the phase portrait of the solution with initial condition near E_1^*. The reason for this is that the stable periodic solution around E_1^* expends as γ increases, and eventually breaks when it meets the second endemic equilibria E_2^* (which has a lower I^* component). As a consequence, a homoclinic bifurcation may occur.

The numerical results mentioned above are for system (7). Simulations suggest that similar behaviours are also present in the full system (4). Figures 9 and 10 illustrate two examples corresponding to Figures 7 and 8, respectively. In Figure 9, all parameter values used are the same as in Figure 7(b) except that $\delta = 0.98$ and $\gamma = 0.46$. It shows that, depending on initial conditions, the solutions may either converge to the stable periodic solution or converge to the DFE. Figure 10 has all parameter value the same as in Figure 8 except that $\delta = 0.99$. It shows similar behaviour as that in Figure 8.

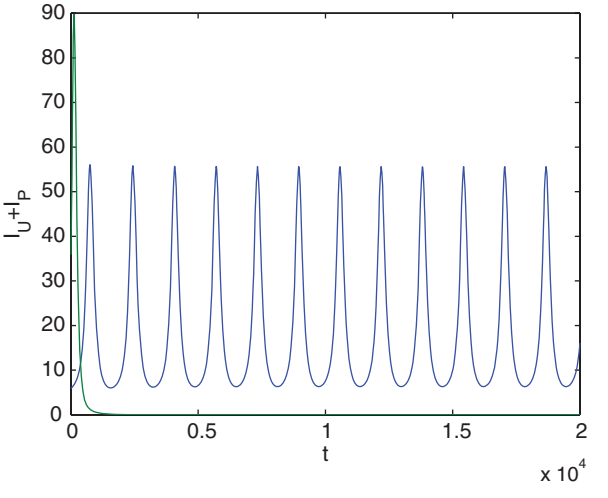

Figure 9. Time plot of the full system (4). All parameter values are the same as in Figure 7 except that $\delta = 0.98$ and $\gamma = 0.46$. $I_U + I_P$ denotes the total number of infectious individuals. It shows that a stable periodic solution exists.

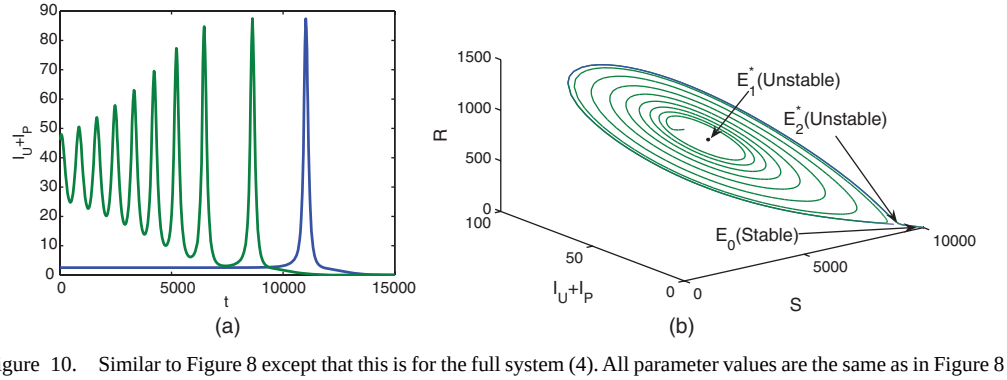

Figure 10. Similar to Figure 8 except that this is for the full system (4). All parameter values are the same as in Figure 8 except that $\delta = 0.99$. $I_U + I_P$ denotes the total number of infectious individuals. It illustrates similar behaviours of solutions to that in Figure 8.

6. Discussion

In this paper, we studied an ordinary differential equation model to explore the effect of the control strategy named 'targeted antiviral prophylaxis' on disease dynamics. Although the model seems to have a similar structure as that of the model in [24, 25], the key differences (besides the fact that their model is structured by the age-since-treatment of uninfected individuals) include the assumption on the infectiousness of individuals who were infected and are being treated, and the assumption on the susceptibility of treated (infected or uninfected) individuals to further infection. It turns out that the disease dynamics predicted by our model have very different qualitative behaviours compared with the model in [24, 25]. More details are provided below.

Most of our analytical results of the model are carried out using the reduced system (7), which assumes that all infectious individuals (with and without treatment) have the same transmission rate (i.e. the assumption that $\delta = 1$) and the same recovery rate (i.e. $\theta = 1$). Under these assumptions, the dimension of the system is reduced to three. We derived threshold conditions that can determine the existence and stability of equilibria and periodic solutions of the system (7). The bifurcation analysis (using γ and f as bifurcation parameters) can be helpful for policymaking. For example, the usual threshold condition for disease control, i.e. $\mathcal{R}_c < 1$, may not be sufficient if the reinfection rate after treatment is sufficiently high (i.e. γ is large). More specifically, when γ is small, the threshold treatment level is f_m (Equation 21) in the sense that disease control is possible when $f > f_m$ (which is equivalent to $\mathcal{R}_c < 1$). However, when γ is large, the disease may still be prevalent even when the treatment level is higher than f_m. In this case, the new threshold level of treatment for disease control is f^* (Equation 27) with $f_m < f^* < 1$.

The results suggest that the system exhibits a *backward* bifurcation in the sense that stable endemic equilibria exist for $\mathcal{R}_c < 1$ (Figure 3). Moreover, depending on parameter values, the system may stabilize at either an endemic equilibrium or an oscillatory state. This is very different from many of the previous results on backward bifurcations in which bistable equilibria are expected (i.e. both the disease-free and an endemic equilibria are stable; see for example, [5–7, 11, 13, 14] and references therein). The possibility of stable periodic solutions for $\gamma < 1$ (and $\mathcal{R}_c < 1$) is also a major difference between our model and that in [24, 25] (when the age-structure is ignored, i.e. when $q(a) = q$ is a constant). The parameter q in their model represents the reduction in susceptibility in treated individuals (who were exposed but not infected), which is similar to the parameter γ in our model (except that our treated non-infectious class P includes those infected individuals whose transmission was blocked by treatment). Their results show that there is at most one endemic equilibrium if $q < 1$, whereas our results show that multiple endemic equilibria are possible when $\gamma < 1$. Although backward bifurcation is not present in [24, 25], numerical studies of our model suggest that, besides the possibility of a stable endemic equilibrium or a stable periodic solution when $\mathcal{R}_c < 1$, there may also exist a homoclinic orbit which connects the unstable and stable manifold of E_2^*.

The main contribution of this study is that it identified the possibility of complex disease dynamics driven by the use of targeted antiviral prophylaxis, provided that the reinfection coefficient (γ) is sufficiently large. It is also demonstrated that, although the usual threshold condition for disease control ($\mathcal{R}_c < 1$) still holds when γ is small (e.g. $\gamma \leq 1/\mathcal{R}_0$), a new threshold quantity, $\mathcal{R}_c^*$ (with $\mathcal{R}_c^* < \mathcal{R}_c$), is required for disease control if γ is large (e.g. $\gamma > 1/\mathcal{R}_0$). That is, if f_m is the critical level of prophylaxis to achieve $\mathcal{R}_c = 1$, the actual threshold level of prophylaxis for disease control (i.e. f^*, for which $\mathcal{R}_c < \mathcal{R}_c^*$) needs to be higher than f_m. If, however, the level f^* is not possible to achieve, then the increase in f must be determined strategically, depending on the goal of the control measure. For example, if oscillatory behaviours in infections are not desirable, then a certain range of f values should be avoided.

Acknowledgements

The authors greatly appreciate the anonymous referees for their valuable comments which help to improve the paper. The research of Qiu is supported by the NSFC grant 10801074 and by the Zijin Star Project of Excellence Plan of NJUST. The research of Feng is supported in part by the NSF grant DMS-0719697.

References

[1] M.E. Alexander and S.M. Moghadas, *Bifurcation analysis of an SIRS epidemic model with generalized incidence*, SIAM J. Appl. Math. 65 (2005), pp. 1794–1816.
[2] M.E. Alexander, S.M. Moghadas, G. Röst, and J. Wu, *A delay differential model for pandemic influenza with antiviral treatment*, Bull. Math. Biol. 70 (2008), pp. 382–397.
[3] M.E. Alexander, C.S. Bowman, S.M. Moghadas, R. Summers, A.B. Gumel, and B.M. Sahai, *A vaccination model for transmission dynamics of influenza*, SIAM J. Appl. Dyn. Syst. 3 (2004), pp. 503–524.
[4] M.E. Alexander, C.S. Bowman, Z. Feng, M. Gardam, S.M. Moghadas, G. Röst, J. Wu, and P. Yan, *Emergence of drug resistance: Implications for antiviral control of pandemic influenza*, Proc. R. Soc. B 274 (2007), pp. 1675–1684.
[5] J. Arino, C.C. Mccluskey, and P. van Den Driessche, *Global results for an epidemic model with vaccination that exhibits backward bifurcation*, SIAM J. Appl. Math. 64 (2003), pp. 260–276.
[6] J. Dushoff, W. Huang, and C. Castillo-Chavez, *Backwards bifurcations and catastrophe in simple models of fatal diseases*, J. Math. Biol. 36 (1998), pp. 227–248.
[7] Z.L. Feng, C. Castillo-Chavez, and A.F. Capurro, *A model for tuberculosis with exogenous reinfection*, Theor. Popul. Biol. 57 (2000), pp. 235–247.
[8] N.M. Ferguson, S. Mallett, H. Jackson, N. Roberts, and P. Ward, *A population-dynamic model for evaluating the potential spread of drug-resistant influenza virus infections during community-based use of antivirals*, J. Anti. Chemo. 51 (2003), pp. 977–990.
[9] N.M. Ferguson, D.A.T. Cummings, C. Fraser, J.C. Cajka, P.C. Cooley, and D.S. Burke, *Strategies for mitigating an influenza pandemic*, Nature 442 (2006), pp. 448–452.
[10] R. Gani, H. Hughes, D. Fleming, T. Griffin, J. Medlock, and S. Leach, *Potential impact of antiviral drug use during influenza pandemic*, Emerg. Infect. Dis. 11 (2005), pp. 1355–1362.
[11] K.P. Hadeler and C. Castillo-Chavez, *A core group model for disease transmission*, Math. Biosci. 128 (1995), pp. 41–55.
[12] F.G. Hayden and F.Y. Aoki, *Amantadine, rimantadine, and relate agents*, in *Antimicrobial Therapy and Vaccines*, V. Yu, T. Meigan, and S. Barriere, eds., Williams and Wilkins, Baltimore, MD, 1999, pp. 1344–1365.
[13] J.F. Jiang and Z.P. Qiu, *The complete classification for dynamics in a nine-dimensional West Nile virus model*, SIAM J. Appl. Math. 69 (2009), pp. 1205–1227.
[14] J.F. Jiang, Z.P. Qiu, J.H. Wu, and H.P. Zhu, Threshold conditions for West Nile virus outbreaks, Bull. Math. Biol. 71 (2009), pp. 627–647.
[15] Y.A. Kuznetsov, *Elements of Applied Bifurcation Theory*, Springer-Verlag, New York, 1995.
[16] M. Lipsitch, T. Cohen, M. Murray, and B.R. Levin, *Antiviral resistance and the control of pandemic influenza*, PLoS Med. 4 (2007), pp. 0111–0120.
[17] W.M. Liu, *Criterion of Hopf bifurcation without using enigenvalues*, J. Math. Anal. Appl. 182 (1994), pp. 250–256.
[18] I.M. Longini, Jr., M.E. Halloran, A. Nizam, and Y. Yang, *Containing pandemic influenza with antiviral agents*, Am. J. Epidemiol. 159 (2004), pp. 623–633.
[19] I.M. Longini, Jr., A. Nizanm, S. Xu, K. Ungchusak, W. Hanshaoworakul, D.A.T. Cummings, and M.E. Halloran, *Containing pandemic influenza at the source*, Science 309 (2005), pp. 1083–1087.
[20] J.M. McCaw and J. McVernon, *Prophylaxis or treatment? Optimal use of an antiviral stockpile during an influenza pandemic*, Math. Biosci. 209 (2007), pp. 336–360.
[21] J.M. McCaw, J.G. Wood, C.T. McCaw, and J. McVernon, *Impact of emerging antiviral drug resistance on influenza containment and spread: Influence of subclinical infection and strategic use of a stockpile containing one or two drugs*, PLoS ONE, 3 (2008), p. e2362, doi:10.1371/journal.pone.0002362.
[22] S. Merler, M. Ajelli, and C. Rizzo, *Age-priortized use of antirvirals during an influenza pandemic*, BMC Infect. Dis. 9 (2009), p. 117.
[23] Z.P. Qiu and Z.L. Feng, *Transmission dynamics of an influenza model with vaccination and antiviral treatment*, Bull. Math. Biol. 72 (2009), pp. 1–33.
[24] H.R. Thieme, A. Tridane, and Y. Kuang, *An epidemic model with post-contact prophylaxis of distributed length. I. Thresholds for disease persistence and extinction*, J. Biol. Dyn. 2 (2008), pp. 221–239.
[25] H.R. Thieme, A. Tridane, and Y. Kuang, *An epidemic model with post-contact prophylaxis of distributed length. II. Stability and oscillations if treatment is fully effective*, Math. Mod. Nat. Phenom. 3 (2008), pp. 267–293.
[26] J. Treanor, *Influenza vaccine-outmaneuvering antigenic shift and drift*, N. Engl. J. Med. 350 (2004), pp. 218–220.